Electronic Supplementary Material (ESI) for ChemComm.

Ultrastable Actinide Endohedral Borospherenes

Cong-Zhi Wang[1], Tao Bo[1], Jian-Hui Lan[1], Qun-Yan Wu[1], Zhi-Fang Chai[1,2], John K. Gibson[3], and Wei-Qun Shi*[1]

[1]Laboratory of Nuclear Energy Chemistry and Key Laboratory for Biomedical Effects of Nanomaterials and Nanosafety, Institute of High Energy Physics, Chinese Academy of Sciences, Beijing 100049, China

*E-mail: shiwq@ihep.ac.cn

[2]School for Radiological and interdisciplinary Sciences (RAD-X) and Collaborative Innovation Center of Radiation Medicine of Jiangsu Higher Education Institutions, Soochow University, Suzhou 215123, China

[3]Chemical Sciences Division, Lawrence Berkeley National Laboratory, Berkeley, California 94720, United States.

Supporting Information

Page 3-4 **Theoretical Methods**

Page 5-7 **Figure S1-S6** Low-lying isomers of AnB_n (An=U, Th, n=36, 38, 40) with the relative energies.

Page 8 **Figure S7** Scalar relativistic MO energy levels for C_{2h} $U@B_{36}$ without and with spin-orbit coupling.

Page 9 **Figure S8** Isosurface plots of spin density and spin polarization parameter function of $U@B_{36}$.

Theoretical Methods

A generalized version of a particle swarm optimization algorithm specific for cluster structure prediction,[1-3] as implemented in Crystal structure AnaLYsis by Particle Swarm Optimization (CALYPSO) code,[1-4] was carried out for global-minimum structural searches for AnB$_n$ (An=U, Th; n=36, 38, 40). The population size (the total number of structures per generation) was set to 40, and the number of generation (the maximum number of generations to be executed for the entire structure prediction simulation) was maintained at 50. Thousands of sampled structures were subjected to evaluation during the structural searches. The structure relaxations were performed using Vienna ab initio simulation package (VASP).[5, 6] The electron exchange-correlation functional was treated using generalized gradient approximation (GGA) in the form proposed by Perdew, Burke and Ernzerhof (PBE).[7] Periodic models were used to model the clusters. A vacuum region of 15 Å was used to isolate finite clusters and prevent interactions between adjacent periodic images. Brillouin zone integration was calculated using gamma point only. The cutoff energy of 450 eV was used in the calculations. All the geometries were optimized until the forces on all the atoms were smaller than 0.04 eV Å^{-1}.

For each of the complexes, the predicted ten energetically low-lying isomers were fully optimized at the hybrid DFT–PBE0 level with the Gaussian 09 program package.[8] For uranium and thorium, the quasi-relativistic effective core potential ECP60MWB and the corresponding valence basis sets ECP60MWB-SEG were used,[9-11] while the 6-311+G(d) basis sets were adopted for boron atoms. This level of theory has been demonstrated as a reliable method for boron clusters, especially for energetics.[12, 13] Given that the highest spin states of the U and Th atoms are quintet and septet, respectively, a series of spin states were considered for each of the U- (singlet, triplet, quintet) and Th-complexes (singlet, triplet, quintet, septet). Meanwhile, the low-lying isomers of each species within 1.0 eV of the global minimum at the PBE0 level, were also optimized by the TPSSh method. Vibrational frequency calculations were carried out to confirm the true minima of the studied structures. The default SCF (self-consistent field) convergence criteria and the default integration grid (75, 302) were used in the calculations. The finer integration grid (120, 974) was used for further evaluating small imaginary vibrational frequencies. Zero-point energy (ZPE) corrections were considered for all the species.

On the basis of the optimized structures, Hirshfeld[14] and Voronoi deformation density (VDD)[15] atomic charges were obtained with the Amsterdam Density Functional program package (ADF 2013.01)[16-18] using PBE0 functional. The Triple-ζ-quality basis sets plus two polarization function (TZ2P)[19] were used with no frozen core approximation considered for all the atoms. Scalar relativistic effects were taken into account by zero-order regular approximation (ZORA)[20]. Spin-orbit (SO) coupling effects on the energy levels were also evaluated with C_{2h} U@B_{36} as a representative complex.

Chemical bonding was elucidated via the quantum theory of atoms-in-molecules (QTAIM)[21-23] and adaptive natural density partitioning (AdNDP)[24] analyses implemented in Multiwfn 3.4 package[25]. The simulated photoelectron spectra were calculated using time-dependent DFT (TD-DFT)[26].

To evaluate the dynamic stabilities of the predicted clusters, the ab initio molecular dynamics (AIMD) simulations within the NVT ensemble were carried out using VASP program package at the temperatures of 300 K and 500 K. Each MD simulation lasted for 30 ps with a time step of 1.0 fs, and the temperatures were controlled by using the Nosé−Hoover method.[27].

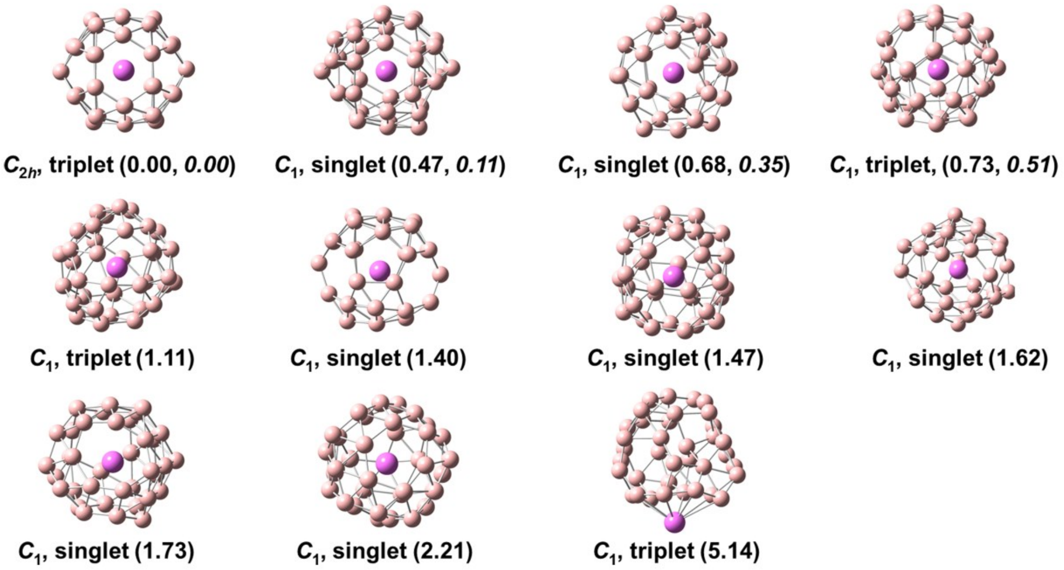

C_{2h}, triplet (0.00, *0.00*) C_1, singlet (0.47, *0.11*) C_1, singlet (0.68, *0.35*) C_1, triplet, (0.73, *0.51*)

C_1, triplet (1.11) C_1, singlet (1.40) C_1, singlet (1.47) C_1, singlet (1.62)

C_1, singlet (1.73) C_1, singlet (2.21) C_1, triplet (5.14)

Figure S1. Low-lying isomers of U@B_{36} with the relative energies (eV) at the PBE0/RECP/6-311+G* and TPSSh/RECP/6-311+G* (*in italic*) levels. Light pink and pink spheres represent B and U, respectively. All the energies have been corrected for zero-point energies.

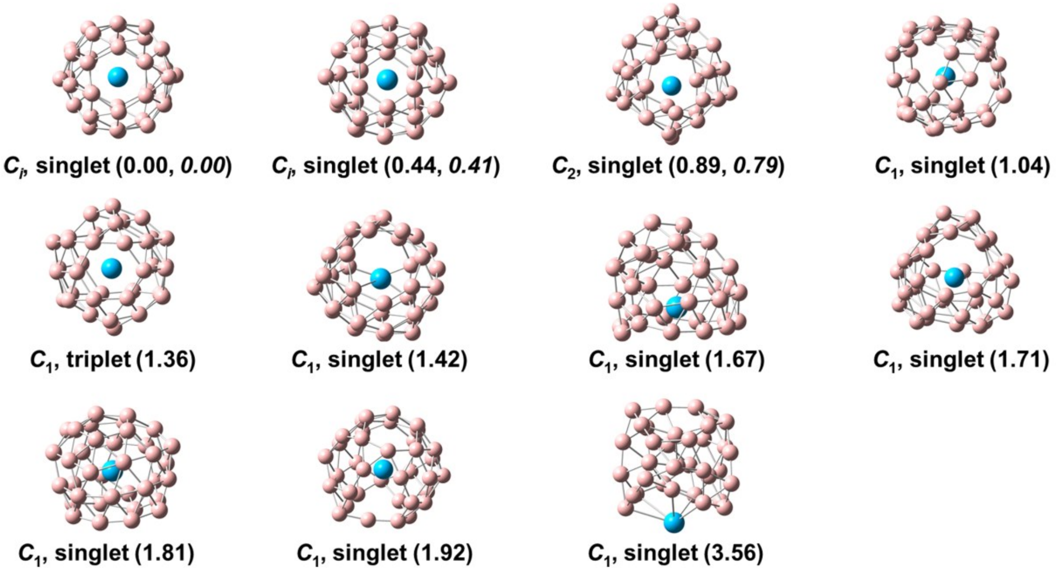

C_i, singlet (0.00, *0.00*) C_i, singlet (0.44, *0.41*) C_2, singlet (0.89, *0.79*) C_1, singlet (1.04)

C_1, triplet (1.36) C_1, singlet (1.42) C_1, singlet (1.67) C_1, singlet (1.71)

C_1, singlet (1.81) C_1, singlet (1.92) C_1, singlet (3.56)

Figure S2. Low-lying isomers of Th@B_{36} with the relative energies (eV) at the PBE0/RECP/6-311+G* and TPSSh/RECP/6-311+G* (*in italic*) levels. Light pink and blue spheres represent B and Th, respectively. All the energies have been corrected for zero-point energies.

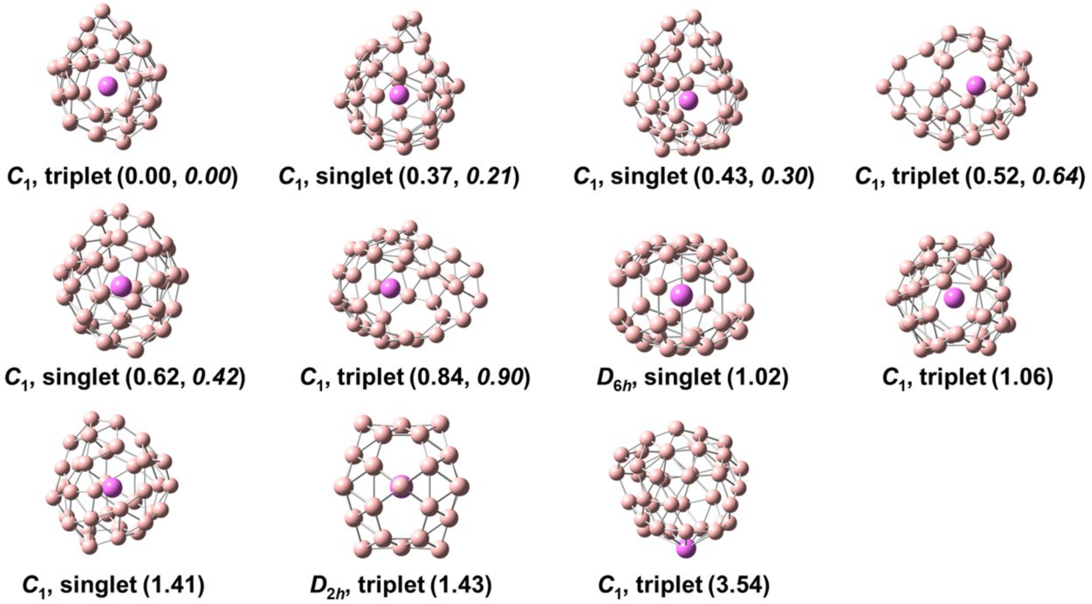

C_1, triplet (0.00, *0.00*)
C_1, singlet (0.37, *0.21*)
C_1, singlet (0.43, *0.30*)
C_1, triplet (0.52, *0.64*)
C_1, singlet (0.62, *0.42*)
C_1, triplet (0.84, *0.90*)
D_{6h}, singlet (1.02)
C_1, triplet (1.06)
C_1, singlet (1.41)
D_{2h}, triplet (1.43)
C_1, triplet (3.54)

Figure S3. Low-lying isomers of U@B_{38} with the relative energies (eV) at the PBE0/RECP/6-311+G* and TPSSh/RECP/6-311+G* (*in italic*) levels. Light pink and pink spheres represent B and U, respectively. All the energies have been corrected for zero-point energies.

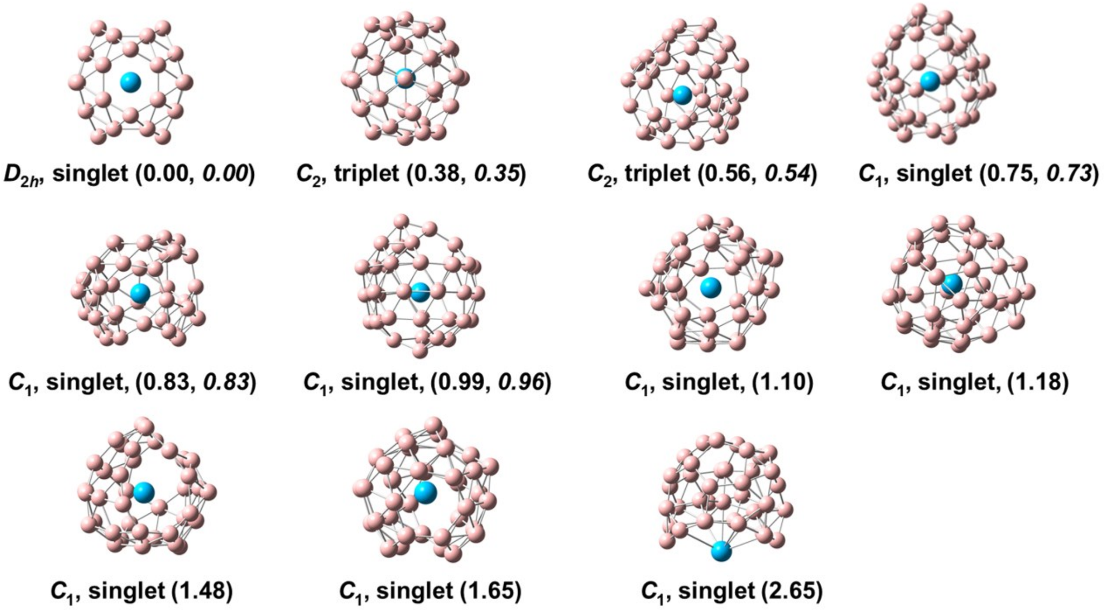

D_{2h}, singlet (0.00, *0.00*)
C_2, triplet (0.38, *0.35*)
C_2, triplet (0.56, *0.54*)
C_1, singlet (0.75, *0.73*)
C_1, singlet, (0.83, *0.83*)
C_1, singlet, (0.99, *0.96*)
C_1, singlet, (1.10)
C_1, singlet, (1.18)
C_1, singlet (1.48)
C_1, singlet (1.65)
C_1, singlet (2.65)

Figure S4. Low-lying isomers of Th@B_{38} with the relative energies (eV) at the PBE0/RECP/6-311+G* and TPSSh/RECP/6-311+G* (*in italic*) levels. Light pink and blue spheres represent B and Th, respectively. All the energies have been corrected for zero-point energies.

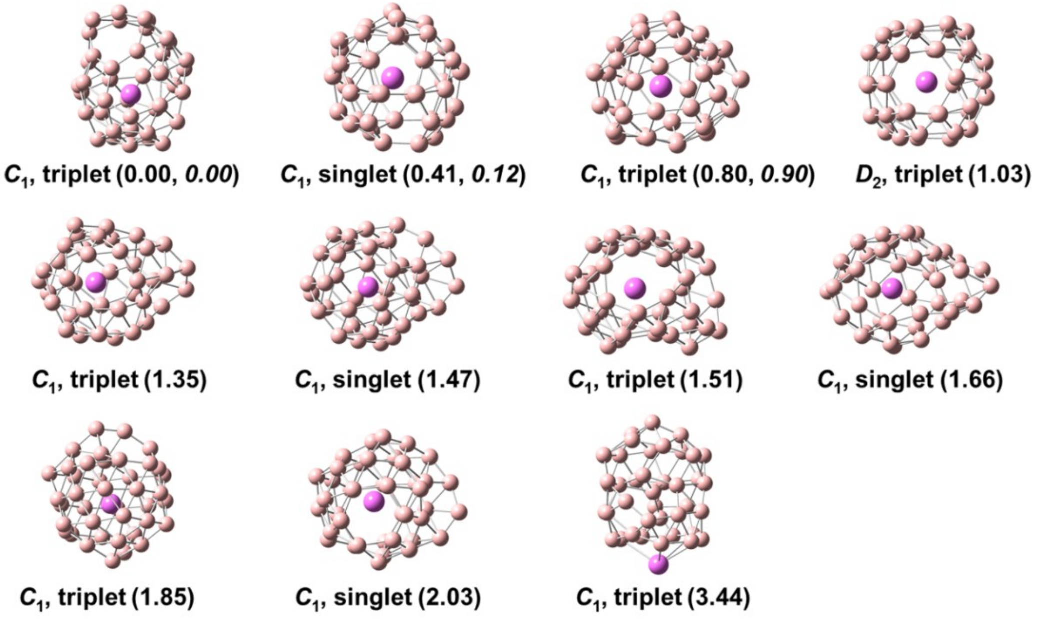

C_1, triplet (0.00, *0.00*) C_1, singlet (0.41, *0.12*) C_1, triplet (0.80, *0.90*) D_2, triplet (1.03)

C_1, triplet (1.35) C_1, singlet (1.47) C_1, triplet (1.51) C_1, singlet (1.66)

C_1, triplet (1.85) C_1, singlet (2.03) C_1, triplet (3.44)

Figure S5. Low-lying isomers of U@B_{40} with the relative energies (eV) at the PBE0/RECP/6-311+G* and TPSSh/RECP/6-311+G* (*in italic*) levels. Light pink and pink spheres represent B and U, respectively. All the energies have been corrected for zero-point energies.

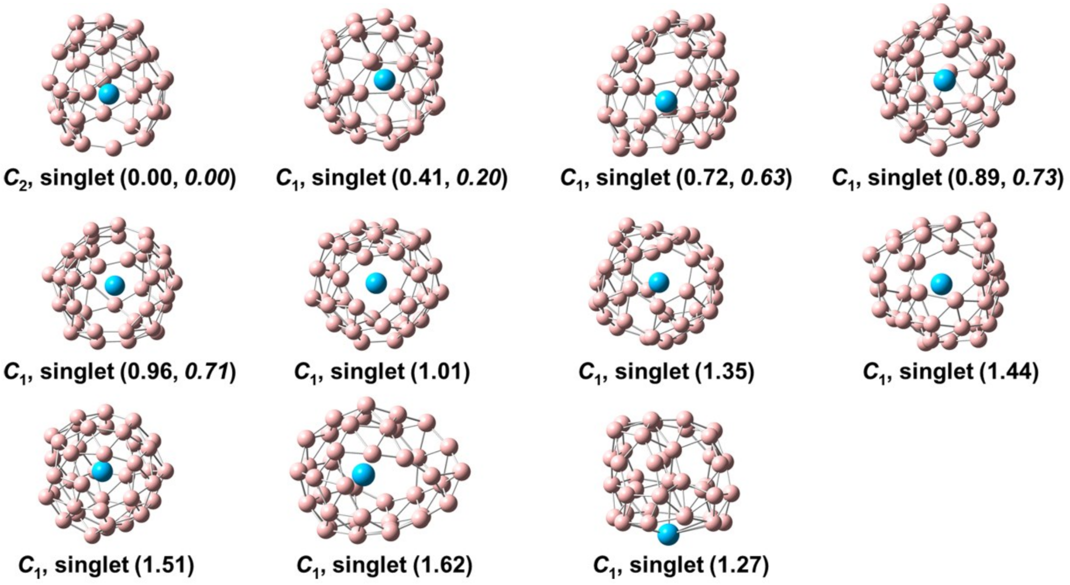

C_2, singlet (0.00, *0.00*) C_1, singlet (0.41, *0.20*) C_1, singlet (0.72, *0.63*) C_1, singlet (0.89, *0.73*)

C_1, singlet (0.96, *0.71*) C_1, singlet (1.01) C_1, singlet (1.35) C_1, singlet (1.44)

C_1, singlet (1.51) C_1, singlet (1.62) C_1, singlet (1.27)

Figure S6. Low-lying isomers of Th@B_{40} with the relative energies (eV) at the PBE0/RECP/6-311+G* and TPSSh/RECP/6-311+G* (*in italic*) levels. Light pink and blue spheres represent B and Th, respectively. All the energies have been corrected for zero-point energies.

Spin-orbit (SO) coupling effect Previous studies[28, 29] on several actinide-centered clusters such as Pu@C_{28} and $[U@Si_{20}]^{6-}$ have shown that the chemical bonding and properties are not sensitive to spin-orbit (SO) coupling. For the studied actinoborospherenes, SO coupling effects on the electronic structures were assessed for the representative complex U@B_{36}. Figure S7 shows the valence orbital energy levels for U@B_{36} with C_{2h} symmetry. As displayed in Figure S7, the MO 39b_u has the largest splitting with the value of about 0.4 eV, which corresponds to the interaction of U 5f orbitals and B 2p orbitals of the cage. The orbital energetic order with SO coupling is found to be similar to that with scalar relativistic effects. Therefore, according to our calculations, the MO splittings are overall small, and the ground-state properties change only slightly due to SO effects.

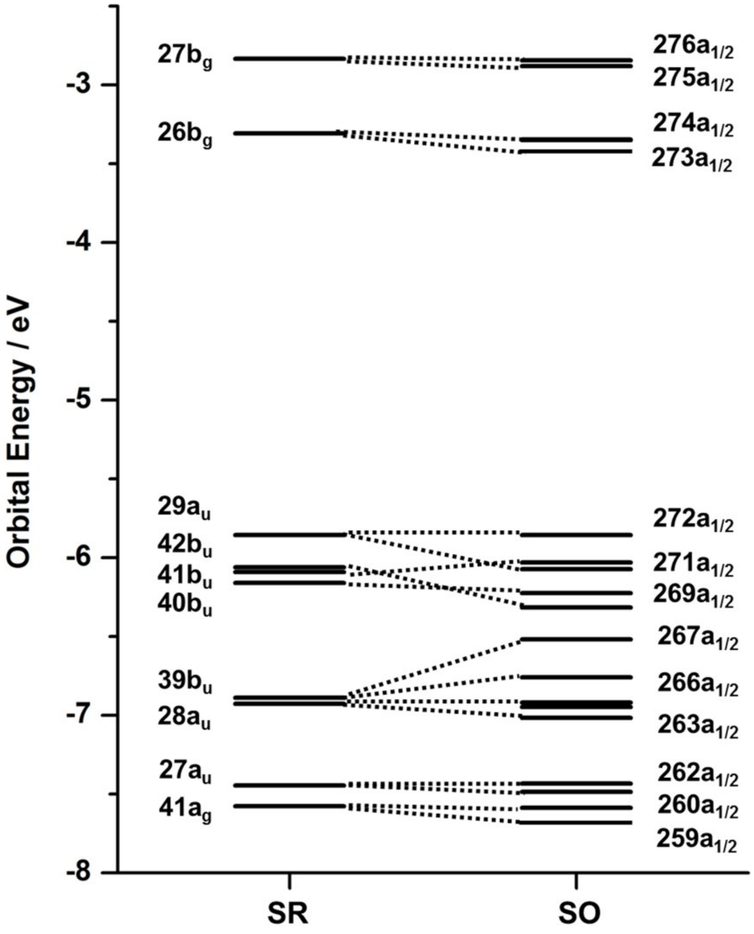

Figure S7. Scalar relativistic (SR) MO energy levels for C_{2h} U@B_{36} without (left) and with (right) spin-orbit (SO) coupling.

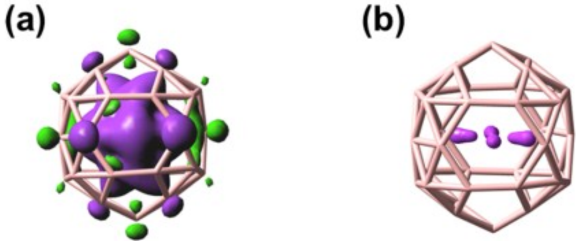

Figure S8. Isosurface plots of (a) spin density (0.002) and (b) spin polarization parameter (0.2, 0.4) function of U@B_{36}.

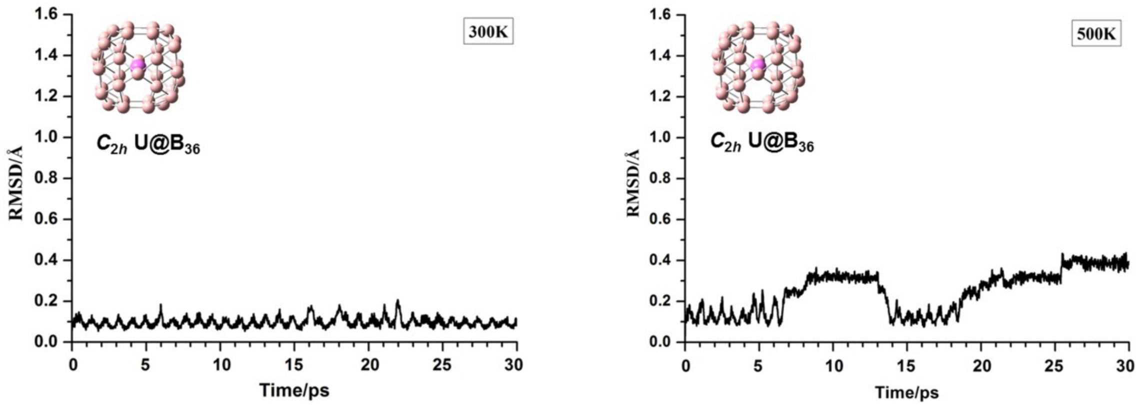

Figure S9. Born-Oppenheimer molecular dynamics simulations of C_{2h} U@B$_{36}$ at 300K and 500K for 30 ps.

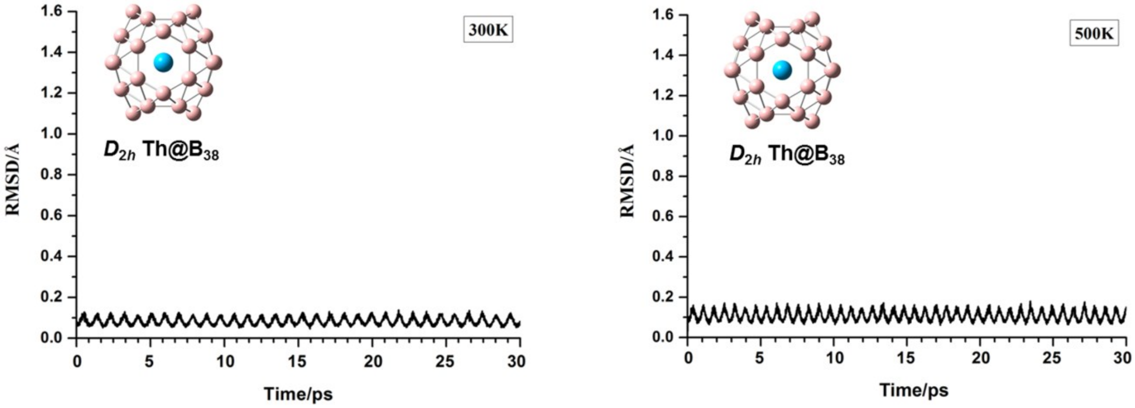

Figure S10. Born-Oppenheimer molecular dynamics simulations of D_{2h} Th@B$_{38}$ at 300K and 500K for 30 ps.

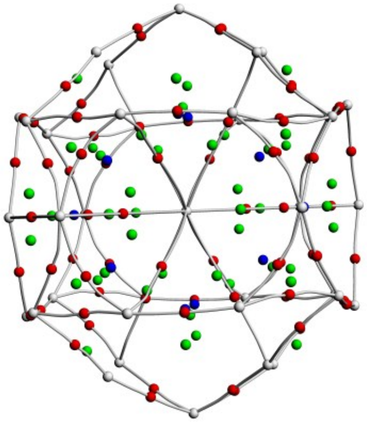

Figure S11. QTAIM molecular graph of C_{2h} U@B$_{36}$. Red points represent bond critical points, gray lines represent bond paths. Green points represent ring critical points, blue points represent cage critical points.

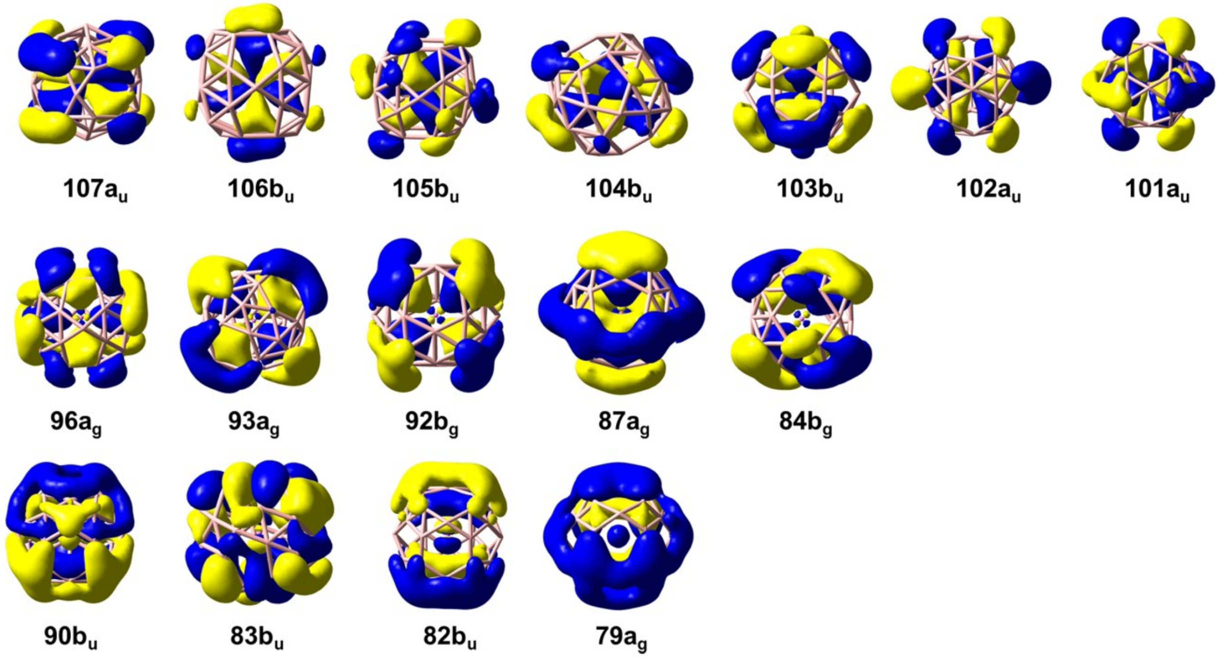

Figure S12. The 16 MOs referring to the 7s, 7p, 6d and 5f electrons from U and 2p orbitals from B in U@B_{36}.

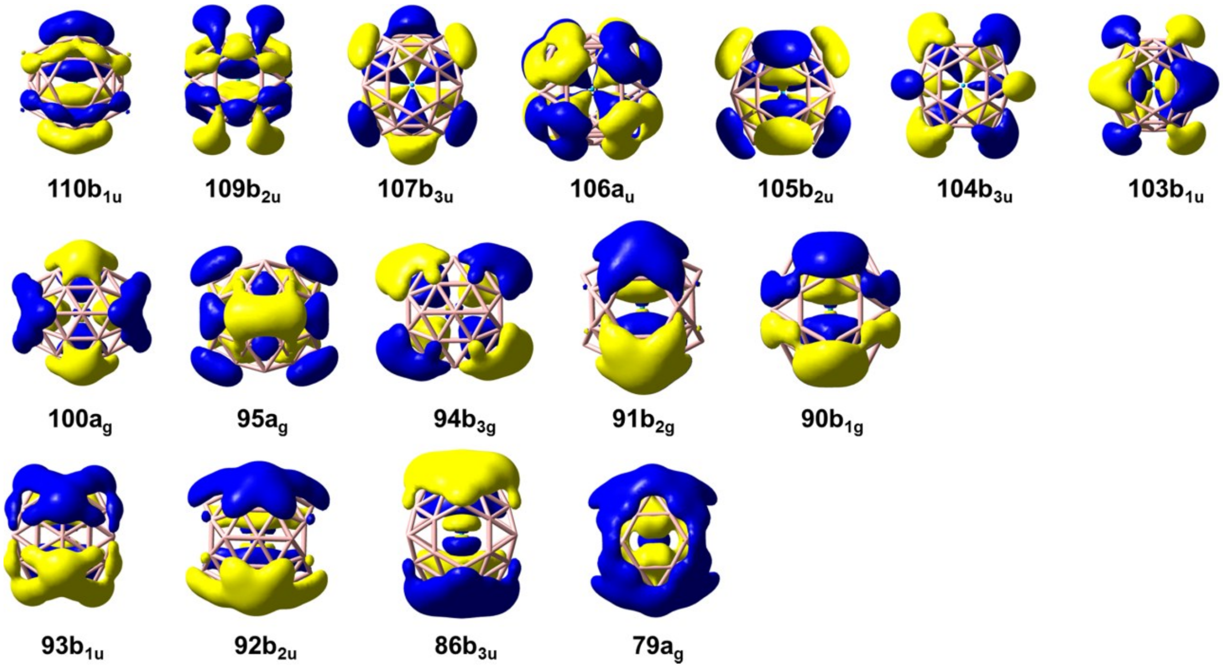

Figure S13. The 16 MOs referring to the 5f, 6d, 7p, and 7s electrons from Th and 2p orbitals from B in Th@B_{38}.

AdNDP analysis of C_{2h} U@B$_{36}$ AdNDP, developed from natural bond orbital (NBO)[30-33] analysis, characterizes the *n*-center two-electron (*n*c–2e) bonding of a molecule with the range of *n* from one up to the total number of atoms in the molecule. Thus, the AdNDP analysis reveals the conventional Lewis bonds (lone pairs and 2c–2e bonds), as well as the nonclassical delocalized bonding (*n*c–2e).

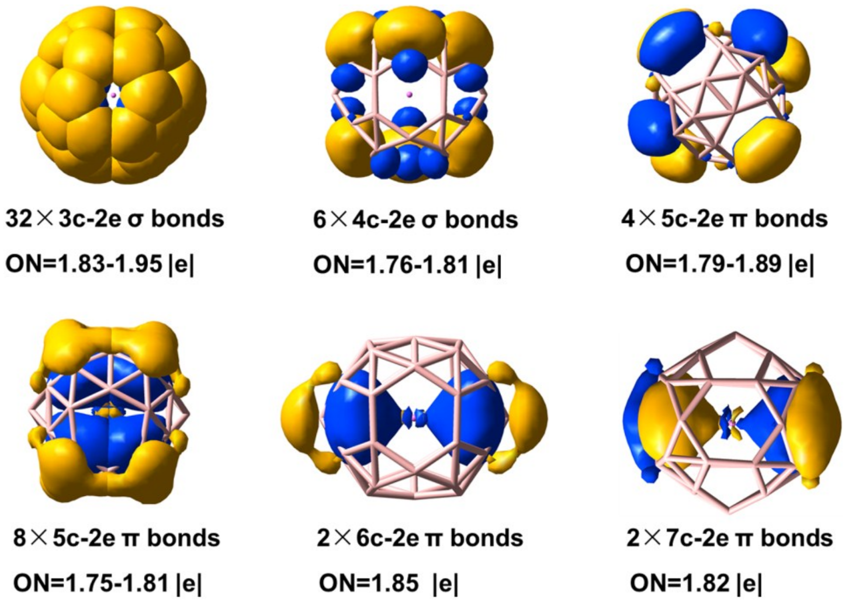

Figure S14. Bonding pattern of the global minimum C_{2h} U@B$_{36}$ from AdNDP analysis with the occupation numbers (ONs) indicated.

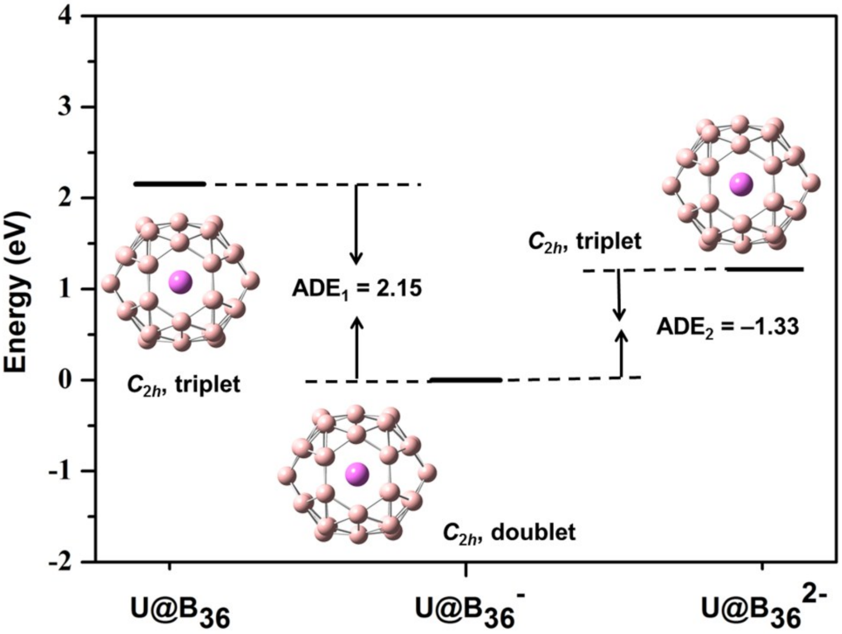

Figure S15. Comparison of the lowest-lying isomers of U@B_{36}, U@B_{36}^{-}, and U@B_{36}^{2-}.

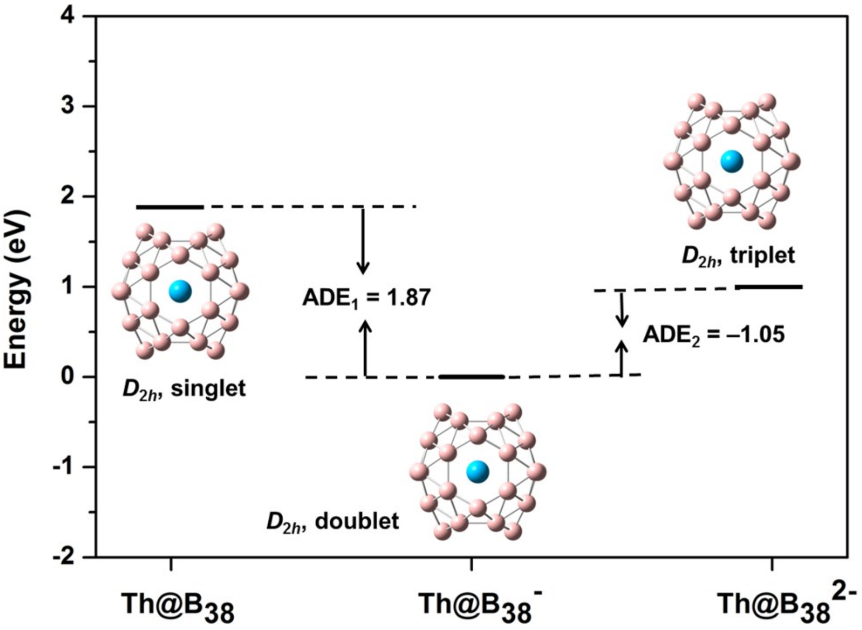

Figure S16. Comparison of the lowest-lying isomers of Th@B_{38}, Th@B_{38}^{-}, and Th@B_{38}^{2-}.

Infrared (IR) absorption spectra To facilitate the future characterizations, we also calculated the IR spectra of C_{2h} U@B$_{36}$ and D_{2h} Th@B$_{38}$. For comparison, the IR spectra of the bare boron cages C_{2h} B$_{36}$ and D_{2h} B$_{38}$ were also predicted. As depicted in Figure S17, there is primarily one IR-active frequency for U@B$_{36}$ (139 cm^{-1}) and Th@B$_{38}$ (121 cm^{-1}), respectively, corresponding to the combined motions of central U, Th atoms and the boron cages, which seems to be at common peculiarity for actinide endohedral borospherenes. Due to the doped actinides, for other IR-active frequencies denoting the motions of the boron cages, the IR spectra peak positions and intensities show some changes for actinide borospherenes as compared to the bare cages. Even so, the main vibrational features of the boron cages are ultimately retained in C_{2h} U@B$_{36}$ and D_{2h} Th@B$_{38}$. For example, the two characteristic peaks of C_{2h} B$_{36}$ at 1327 and 811 cm^{-1} are slightly red-shifted toward C_{2h} U@B$_{36}$ (1306 and 792 cm^{-1}). These results make it possible to establish that the structural and chemical, as well as spectroscopic integrities of the C_{2h} B$_{36}$ and D_{2h} B$_{38}$ cages are basically maintained in these actinide endohedral borospherenes.

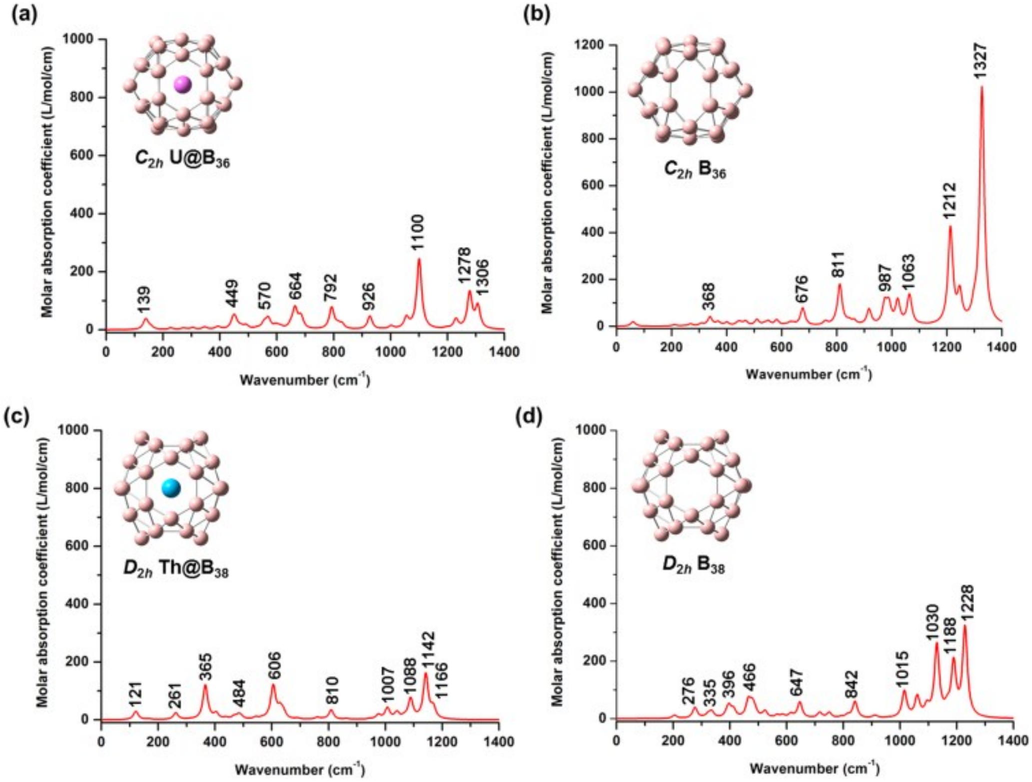

Figure S17. Simulated photoelectron spectrum of (a) C_{2h} U@B$_{36}^{-}$ and (b) D_{2h} Th@B$_{38}^{-}$ at the PBE0/RECP/6-311+G* level of theory.

Table S1. Topological parameters for the U−B bond critical points (BCPs) of C_{2h} U@B$_{36}$

U-B BCPs	ρ	$\nabla^2\rho$	H(r)	ELE	LOL
1	0.0407	0.0785	-0.0072	0.2119	0.3410
2	0.0376	0.0646	-0.0063	0.2259	0.3506
3	0.0356	0.0800	-0.0048	0.1667	0.3089
4	0.0462	0.0635	-0.0102	0.2996	0.3954
5	0.0407	0.0785	-0.0072	0.2119	0.3410
6	0.0376	0.0646	-0.0063	0.2259	0.3506
7	0.0376	0.0646	-0.0063	0.2259	0.3506
8	0.0407	0.0785	-0.0072	0.2119	0.3410
9	0.0462	0.0635	-0.0102	0.2996	0.3954
10	0.0376	0.0646	-0.0063	0.2259	0.3506
11	0.0407	0.0785	-0.0072	0.2119	0.3410
12	0.0356	0.0800	-0.0048	0.1667	0.3089

Table S2. Calculated compositions (%) of the frontier molecular orbitals of U@B_{36}.

MOs		U			
		5f	6d	7p	7s
109	LUMO+1		8.7		
108	LUMO		1.8		
107	SOMO	26.8		1	
106	SOMO-1	75.7		3	
105	HOMO	52.3			
104	HOMO-1	60.9			
103	HOMO-2	28.8			
102	HOMO-3	15.4			
101	HOMO-4	15.2			
100	HOMO-5		2.0		
96			15.1		
93			17.6		
92			16.6		
90				2.8	
87			17.1		
84			15.4		
83				8.3	
82				4.0	
79					3.8

Table S3. Calculated compositions (%) of the frontier molecular orbitals of Th@B_{38}.

MOs		Th			
		5f	6d	7p	7s
112	LUMO+1		2.4		
111	LUMO		6.0		
110	HOMO	19.3			
109	HOMO-1	9.8			
108	HOMO-2		1.8		
107	HOMO-3	17.5			
106	HOMO-4	14.1			
105	HOMO-5	11.7			
104	HOMO-6	8.2			
103	HOMO-7	8.4			
102	HOMO-8				
100			16.9		
95			12.6		
94			16.3		
93				4.7	
92				6.8	
91			17.7		
90			16.2		
86				7.0	
79					3.3

References

1. J. Lv, Y. C. Wang, L. Zhu and Y. M. Ma, *J. Chem. Phys.*, 2012, **137**, 084104-084111
2. Y. C. Wang, J. Lv, L. Zhu and Y. M. Ma, *Comput. Phys. Commun.*, 2012, **183**, 2063-2070.
3. Y. C. Wang, J. A. Lv, L. Zhu and Y. M. Ma, *Phys Rev B*, 2010, **82**, 094116-094123.
4. Y. C. Wang, M. S. Miao, J. Lv, L. Zhu, K. T. Yin, H. Y. Liu and Y. M. Ma, *J. Chem. Phys.*, 2012, **137**, 224108-224113.
5. G. Kresse and J. Hafner, *Phys Rev B*, 1993, **48**, 13115-13118.
6. G. Kresse and J. Furthmuller, *Phys Rev B*, 1996, **54**, 11169-11186.
7. J. P. Perdew, K. Burke and M. Ernzerhof, *Phys. Rev. Lett.*, 1996, **77**, 3865-3868.
8. M. J. Frisch, G. W. Trucks, H. B. Schlegel, G. E. Scuseria, M. A. Robb, J. R. Cheeseman, G. Scalmani, V. Barone, B. Mennucci, G. A. Petersson, H. Nakatsuji, M. Caricato, X. Li, H. P. Hratchian, A. F. Izmaylov, J. Bloino, G. Zheng, J. L. Sonnenberg and M. Hada, Ehara, M.; et al., *Journal*, 2009.
9. W. Kuchle, M. Dolg, H. Stoll and H. Preuss, *J. Chem. Phys.* , 1994, **100**, 7535-7542.
10. X. Y. Cao and M. Dolg, *J. Molec. Struct. (THEOCHEM)* 2004, **673**, 203-209.
11. X. Y. Cao and M. Dolg, *J. Molec. Struct. (THEOCHEM)* 2002, **581**, 139-147.
12. F. Y. Li, P. Jin, D. E. Jiang, L. Wang, S. B. B. Zhang, J. J. Zhao and Z. F. Chen, *J. Chem. Phys.*, 2012, **136**, 074302.
13. H. Bai, Q. Chen, C. Q. Miao, Y. W. Mu, Y. B. Wu, H. G. Lu, H. J. Zhai and S. D. Li, *Phys. Chem. Chem. Phys.*, 2013, **15**, 18872-18880.
14. F. L. Hirshfeld, *Theor. Chim. Acta*, 1977, **44**, 129-138.
15. C. F. Guerra, J. W. Handgraaf, E. J. Baerends and F. M. Bickelhaupt, *J. Comput. Chem.*, 2004, **25**, 189-210.
16. Y. Q. Zhang, C. L. Luo and Z. Yu, *Int J Mod Phys B*, 2005, **19**, 2538-2543.
17. Y. Q. Zhang, C. L. Luo and Z. Yu, *Int. J. Quantum Chem.*, 2005, **102**, 165-173.
18. S. Yamanaka and K. Yamaguchi, *Bull. Chem. Soc. Jpn.*, 2004, **77**, 1269-1286.
19. A. Harju, E. Rasanen, H. Saarikoski, M. J. Puska, R. M. Nieminen and K. Niemela, *Phys Rev B*, 2004, **69**.
20. Y. Q. Zhang, C. L. Luo and Z. Yu, *New J. Chem.*, 2005, **29**, 1285-1290.
21. R. F. W. Bader, *Atoms in Molecules: A Quantum Theory*, Oxford University Press, Oxford, U.K., 1990.

22. R. F. W. Bader, *J. Phys. Chem. A* 1998, **102**, 7314-7323.

23. R. F. W. Bader, *Chem. Rev.* , 1991, **91**, 893-928.

24. D. Y. Zubarev and A. I. Boldyrev, *Phys. Chem. Chem. Phys.*, 2008, **10**, 5207-5217.

25. T. Lu and F. W. Chen, *J. Comp. Chem.* , 2012, **33**, 580-592.

26. R. Bauernschmitt and R. Ahlrichs, *Chemical Physics Letters*, 1996, **256**, 454-464.

27. G. J. Martyna, M. L. Klein and M. Tuckerman, *J. Chem. Phys.*, 1992, **97**, 2635-2643.

28. J. P. Dognon, C. Clavaguera and P. Pyykkö, *J. Am. Chem. Soc.*, 2009, **131**, 238-243.

29. J. P. Dognon, C. Clavaguera and P. Pyykkö, *Chem Sci*, 2012, **3**, 2843-2848.

30. J. E. Carpenter and F. Weinhold, *J. Mol. Struct. (THEOCHEM)*, 1988, **169**, 41-62.

31. J. P. Foster and F. J. Weinhold, *J. Am. Chem. Soc.* , 1980, **102**, 7211-7218.

32. A. E. Reed, R. B. Weinstock and F. Weinhold, *J. Chem. Phys.* , 1985, **83**, 735-746.

33. A. E. Reed, L. A. Curtiss and F. Weinhold, *Chem. Rev.* , 1986, **6**, 899-926.